Organic solar cells: study of combined effects of active layer nanostructure and electron and hole transport layers

HASSAN, Aseel <http://orcid.org/0000-0002-7891-8087>, KADEM, Burak and CRANTON, Wayne <http://orcid.org/0000-0002-0142-7810>

Organic solar cells: study of combined effects of active layer nanostructure and electron and hole transport layers

Aseel Hassan, Burak Kadem and Wayne Cranton
Material and Engineering Research Institute, Sheffield Hallam University
Howard Street, S1 1WB Sheffield, UK

Abstract:
An organic solar cell based on Poly (3-hexathiophine-2,5-diyl) and [6,6]-Phenyl C_{61} butyric acid methyl ester has been subjected to all layers treatment and was investigated for combined effects of the these layers on device performance. These treatment included optimization of active layer morphology and thickness and improving the structure of the hole and electron transport layers, as well as subjecting the full device to optimum post deposition thermal treatment. Such a device has shown an increase in the optical absorption intensity in the near infrared region compared to the reference device, which is thought to be advantageous for producing high current density. The increase in the current density has also been correlated with light trapping within the active layer and the possibility of the occurrence of total internal reflection, which was explained using total internal reflection spectroscopic ellipsometry measurements. The current density-voltage characteristics have been measured in dark and under illumination. Power conversion efficiency as high as 7% has been achieved correlated with a fill factor of 71%.

Keywords: Organic solar cell; P3HT:PCBM; Light trapping and scattering; Total internal reflection

1. Introduction

Organic materials have played a significant role in the field of optoelectronic applications due to their simple device processing on flexible substrates as well as possible large scale production using role-to-role technology [1-5]. Several investigations have been carried out during the last few years in order to produce highly efficient organic solar cells (OSCs) addressing different challenges, mainly device performance and stability through the control of active morphology [6-9]. This property has demonstrated a significant influence on the orientation of the organic molecules within the blend, which directly impacts on charge carriers' transfer [10]. Active layer

morphology also directly affect the interfaces between the two system components within the Poly (3-hexathiophine-2,5-diyl) (P3HT) and [6,6]-Phenyl C_{61} butyric acid methyl ester (PCBM) blend, which in turn influences the charge carriers' separation [10]. Furthermore, the metal-semiconductor contact, as well as the energy offset between the donor and the acceptor levels, is another essential parameter which influences the overall performance of the OSCs [10]. Up-to-date, the highest performance OSC has been reported by Toshiba with power conversion efficiency (PCE) of 11±0.3% [11]. Among all the organic materials, P3HT:PCBM blends are the most investigated organic system for OSC applications; the highest recorded PCE for this system is found to be in the range of 4.5-6% [12-14]. Recently, we have reported several approaches based on different treatments of blends comprising P3HT:PCBM; these include, employing cosolvents to dissolve the active layer materials [15, 16] with highest PCE recorded for a cosolvents treatment of chlorobenzene (CB):chloroform (CF) (1:1) is 2.73%. Further investigation was carried out to optimise active layer thickness where the highest PCE of 3.86% was associated with a layer thickness of 95nm [17]. We have also utilised different fullerene derivatives to control the open circuit voltage of the OSCs; a PCE of 4.2% was reported for OSC active layer to blend comprising P3HT:PC_{61}BM [18]. Moreover, post-annealing treatment of P3HT:PCBM devices have been shown to play an important role if determining device characteristics; an optimum PCE of 5.5% was found for OSC devices treated at 140 ^{o}C [10]. Using soluble Alq3 compound as an electron transport layer (ETL) [19] to modify the aluminium (Al) back contact, an improved PCE of 3.92% was achieved without post-annealing treatment for the P3HT:PCBM blend. In a final attempt to improve the performance of the OSC of this study, the poly(3,4-ethylenedioxythiophene)-poly(styrenesulfonate) (PEDOT:PSS) hole transport layer (HTL) has been doped with different metal salts, which include lithium chloride (LiCl), cadmium chloride ($CdCl_2$), sodium chloride (NaCl) and copper chloride ($CuCl_2$) in solution forms. It has been concluded that PEDOT:PSS treated with LiCl solution (10 mg.ml^{-1}) has resulted in the most improved P3HT:PCBM-based device performance with PCE of 6.82% [20].

In the current study, all the device processes described above are applied in one process in order to investigate the combined effects of the same device; the final configuration of such process is summarised in Fig. 1.

2. Experimental details

2.1. Sample preparation

P3HT, PCBM, PEDOT:PSS (1.3 wt% dispersion in H_2O, conductive grade), CB, CF, tris-(8-hydroxyquinoline) Aluminium (Alq3) were purchased from Sigma-Aldrich and used without any further purification. Devices were fabricated using indium tin oxide (ITO) coated glass slides with a sheet resistance of 8-12 Ω/□ from the same supplier. P3HT:PCBM active layer processing, the PEDOT:PSS as hole transport layer treatment and Alq3 as electron transport layer have been prepared following procedures described in our previous publications [10, 15-20]. For the reference device PEDOT:PSS was spun onto ITO slides and annealed at 150 ^{o}C for 10 min in ambient air, whereas for the completely processed devices PEDOT:PSS layers were doped with metal salts prior to annealing at 150 ^{o}C [20]. P3HT:PCBM active layer in the ratio 1:1 (14 mg.ml^{-1}) were dissolved in cosolvents of CB:CF with the ratio of 1:1. The active layers were spin coated inside a nitrogen-filled glove box followed by annealing inside the glove box at 120 ^{o}C for 10 min. Film thickness of about 100 nm was obtained as determined by spectroscopic ellipsometry. In the case of the completely processed devices and prior to evaporating aluminium (Al) top contact of 100 nm thickness, Alq3 was spin coated as ETL onto the active layer [19]; the examined OSCs have a device active area of 0.07 cm^2. Except for the reference device all the fully processed devices were subjected to further heat treatment inside the glove box at 140 ^{o}C for 10 min and left to cool down for 30 min before measurements were carried out. An average of three devices has been used to carry out error analysis.

2.2. Characterization techniques

UV-visible spectrophotometer (Varian 50-scan UV-visible) in the range of 190-1100 nm has been used to study the absorption and transmittance spectra of the studied layers. The films' morphology has been investigated using a Nanoscope IIIa multimode (Bruker) atomic force microscope (AFM) and an FEI-Nova scanning electron microscope (SEM). The Mott-Schottky analysis was employed to study the capacitance versus voltage (C-V) characteristics of the OSC devices using an HP4284A (20 Hz-1 MHz) Precision LCR meter; discussion of the theoretical part of this analysis is found elsewhere [10]. The photovoltaic (PV) properties were studied using a 4200 Keithley semiconductor characterization system and the photocurrent was generated under AM 1.5 solar simulator source of 100 mW.cm^{-2}. The Fill factor (FF) and the PCE of the solar cells were evaluated using the following equations [21]:

$$PCE\ (\%) = \frac{J_{max}\ V_{max}}{P_{in}} \quad (1)$$

$$FF = \frac{J_{max}\ V_{max}}{J_{sc}\ V_{oc}} \quad (2)$$

where J_{sc} is the short circuit current density ($mA.cm^{-2}$), V_{oc} is the open-circuit voltage (V), P_{in} is the incident light power and J_{max} ($mA.cm^{-2}$) and V_{max} (V) are the current density and voltage at the point of maximum power output in the current density versus voltage (J-V) curves, respectively.

3. Results and discussions

3.1. Optical properties:

Fig. 2 shows the absorption and transmittance spectra for the layers under study as well as the complete device (without Al electrode). Generally, Alq3 layer has exhibited typical transmittance spectra with an optical band gap of 2.83 eV [16]. PEDOT:PSS treated with LiCl metal salt has shown lower transmittance in the near infrared (NIR) region compared to the visible region; this could be related to the absorption of the PEDOT:PSS layer within this region. Gasiorowski and co-authors have reported that PEDOT:PSS layer has a small absorption coefficient in the UV and visible regions, while it has a higher absorption coefficient in the NIR region of the spectra [22]. P3HT:PCBM active layer, on the other hand, has shown 4 different bands (a,b,c and d); bands a, b and c were attributed to the P3HT absorption, while band d was ascribed to the absorption of PCBM molecules [15]. Similar spectra have been observed for the complete device structure (before depositing the Al back contact) correlated with an increase in the absorption intensity over the investigated spectral range and a clear absorption enhancement in the NIR region as well as in the UV region (below 400 nm). The absorption band d has almost diminished and became as a shoulder on the latter peak. The absorption enhancement in the fully-treated device could be ascribed to the contribution of absorption of the salt-treated PEDOT:PSS layer within the complete device [22] and/or the light scattering and trapping within the complete device [23]. The surface roughness of ITO/LiCl-treated PEDOT:PSS layer could result in light scattering, therefore it may contribute in longer light propagation pathway within the P3HT:PCBM active layer and results in light trapping. Generally, light trapping occurs due to total internal reflection (TIR), absorption, and surface plasmon. Increasing the optical path length within a device by light trapping supports the light bouncing back and forth about 50 times [24]. The proposed light

trapping mechanism is depicted in Fig. 3 showing the scattered light from the ITO/LiCl-treated PEDOT:PSS layer. Surface morphology of the PEDOT:PSS layer is illustrated using a SEM image, as shown in Fig. 4, whereas its surface roughness has been investigated using AFM image as shown in Fig. 5. Light scattering and trapping within the complete device are thought to be beneficial in enhancing light harvesting by the device active layer and therefore increasing the current density and subsequently device efficiency [23, 25]. Petoukhoff and co-workers have stated that roughness of the absorber layer assists in light scattering [26], a property which is thought to contribute to increasing the light absorption leading to increased current density. The same authors have also demonstrated an overall absorption enhancement as large as 12% in organic semiconductor layers with different metal coated glass substrates. It has also been verified that total absorption might be further improved by minimising reflection losses when the polymer/fullerene active layer is incorporated into a complete device which incorporates charge transport layers on both sides of the device as well as an anti-reflection layer [26]. Another possibility of enhancing light propagation through the device is through the reflected light from the randomly textured organometallic/metal electrode (Alq3/Al) to the P3HT:PCBM active layer, as defined by the Lambertian limit, where the reflected light exhibits prolonged optical path [27]. Randomising the direction of light may assist the reflected light to be totally internally reflected, where in the present case, the light reaching the Alq3/Al surface at an angle higher than the critical angle will be totally reflected towards the active layer, leading to dramatic improvement in light absorption [27-29].

A further reason that might enhance optical absorption by the active layer is due to possible surface plasmon resonance (SPR) at the interface between ITO/PEDOT:PSS and the active layer. Initial measurements using total internal reflection-enhance spectroscopic ellipsometry (TIRE) has been carried out using J.A.Woollam (M2000) spectroscopic ellipsometer. This technique measures two angles, Ψ and Δ, which are defined as the ratio of complex reflection coefficients (ρ) of the two electric components, *p* (parallel) and *s* (normal) to the plane of incidence and Δ is the phase shift between the two polarised light components, respectively [30]. Utilising a prism of the angle of 68^{o} the measured spectra have shown two resonance minima at 660 nm and 850 nm due to possible SPR phenomena at the above-mentioned interface [31] as shown in Fig. 6. These results are the subject of further investigation in order to elucidate the exact origin of these spectra. A similar observation has been reported by Baba and co-authors in P3HT:PCBM blends based on grating-coupling SPR [32].

3.2. Electrical properties

The performance of the complete device has been investigated in the dark and under AM 1.5 solar simulator source of 100 mW.cm^{-2}. Fig. 7 shows the J-V characteristics of the investigated solar cells, demonstrating best device characteristics. The derived PV parameters of three different devices are summarised in Table 1 with an average PCE of 6.95%, and an average FF of 70%. The further increase in light absorption in the NIR region in the complete device may have resulted in a higher current density of 16.2 mA.cm^{-2} in comparisons to the reference device [17]. However, J_{sc} decrement from 17.97 mA.cm^{-2} in the device with PEDOT:PSS doped with metal salts [17] to 16.2 mA.cm^{-2} in the completely processed device might be ascribed to the energy level mismatch between the active layer and Alq3 layer [33]. Furthermore, controlling the polymer nanoscale and enhancing the organic phase-separation of P3HT:PCBM active layer could improve J_{sc} and FF and hence the good PCE [34]. According to Shockley-Queisser limit (SQL) which establishes a theoretical limit for FF as a function of V_{oc}, the FF in OSCs is expected to be lower than that for inorganic solar cells counterpart due to possible increased charge recombination [35, 36]. An improved heterojunction is desirable for excitons' dissociation into free charge carriers where an additional energy is required; therefore, the OSC efficiency is thought to be lower than the SQL. This extra energy ultimately leads to a decreased open circuit voltage [37, 38]. However, the short circuit current density of the OSC can possibly exceed that for a single p–n junction inorganic solar cell due to the effect of singlet exciton fission when one photon can produce two pairs of electrons and holes [39].

The analysis of the studied device was further carried out using dark J-V and C-V measurements. The barrier height (ϕ_B) and the ideality factor (n) of the devices were determined using the following equations [40, 41]:

$$\phi_B = \frac{kT}{q} \ln\left(\frac{A^*T}{J_o}\right) \quad (1)$$

$$n = \frac{q}{kT}\left(\frac{dV}{d\ln J}\right) \quad (2)$$

where q is the fundamental electron charge, k is Boltzmann constant, T is the absolute temperature, and A^* and J_o are the Richardson constant (120 mA cm^{-2} K^{-2}) and the reverse saturation current density, respectively. The theoretical background for C-V measurements analysis can be found elsewhere [10]. The ideality factor with a value of 1.6 was estimated from

the dark characteristics presented in the inset of Fig. 7; this value indicates that lower recombination rate occurs within the device which could be assigned to the effective charge collection from the respected electrodes by employing efficient hole and electron transport layers [19, 20]. The efficient charge collection contributes in the high FF obtained in the current work [42]. The noticeable increase in the J_{sc} is consistent with the increase in internal power conversion efficiency (IPCE) measurements as shown in Fig. 8. The latter data shows a typical spectral response of P3HT:PCBM blend with a maximum IPCE of about 40% at 520 nm. The increase in the spectral response of the completely processed device by about 50% above the pristine reference device is consistent with the increase in the short circuit current [43]. Furthermore, Schottky barrier is created and a depletion region is formed when the P3HT:PCBM blend is contacted with a low work function metal contact [44]. On the other hand, the anode (ITO/PEDOT:PSS) is considered as an ohmic contact because of the energy level alignment between the PEDOT:PSS and P3HT [10, 45]. The barrier height of 0.86 eV (as shown in Table 1) has been estimated from the J-V characteristics. The built-in potential (V_{bi}) can be estimated from the extrapolation of the linear part intersection with the voltage axis of the dC^{-2}/dV plot shown in Fig. 9; this gives a value of V_{bi}=0.52 eV and the estimated ϕ_B is 0.86 eV which is in agreement with the value derived in this work from the dark J-V characteristics. Furthermore, the series resistance of 45 Ω was estimated using the dark J-V measurement which is thought to enhance the device FF [45]. It is well-known that FF represents the efficiency of charge collection before they recombine inside the cell which basically depends on the charge carrier's mobility, the built-in potential and the carrier recombination rate [46]. FF as high as 71% has been calculated which is one of the highest reported values in OSCs [45, 47, 48].

Conclusion:

P3HT:PCBM-based solar cells have been examined in a completely processed device structure with a configuration of ITO/LiCl-treated-PEDOT:PSS/P3HT:PCBM/Alq3/Al. This novel configuration structure has evidenced a remarkable improvent in the OSC device performance as well as an increase in the optical absorption intensity in the NIR region leading to enhanced IPCE in about 50% compared to the reference device. The device has shown a significant enhancement in the PV performance compared to the reference device with PCE of 7%, FF of 71%, V_{oc} of 0.61 V and J_{sc} of 16.2 $mA.cm^{-2}$. The PCE enhancement has been attributed to the increase in J_{sc}; the latter was attributed to the absorption enhancement in the fully-treated device

which could be ascribed to the contribution of absorption of the salt-treated PEDOT:PSS layer within the complete device, the light scattering and trapping within the complete device, and/or the total internal reflection of light. Moreover, the efficient electron and hole transport layers are thought to have contributed to efficient charge collection which results in improved FF.

Acknowledgment:

One of the authors (BK) would like to acknowledge his study sponsorship from the Iraqi Ministry of higher Education and Scientific Research, and Babylon University, Faculty of Science, Department of Physics.

References:

[1] T. Da Ros, M. Prato, M. Carano, P. Ceroni, F. Paolucci, S. Roffia, L. Valli and D. Guldi, Synthesis, electrochemistry, Langmuir–Blodgett deposition and photophysics of metal-coordinated fullerene–porphyrin dyads. Journal of Organometallic Chemistry, 599 (2000) 62-68.

[2] S. Conoci, D. Guldi, S. Nardis, R. Paolesse, K. Kordatos, M. Prato, G. Ricciardi, M.G.H Vicente, I. Zilbermann and L. Valli, Langmuir–Shäfer Transfer of Fullerenes and Porphyrins: Formation, Deposition, and Application of Versatile Films. Chemistry–A European Journal, 10 (2004) 6523-6530.

[3] D. Guldi, I. Zilbermann, G.A. Anderson, K. Kordatos, M. Prato, R. Tafuro and L. Valli, Langmuir–Blodgett and layer-by-layer films of photoactive fullerene–porphyrin dyads. Journal of Materials Chemistry, 14 (2004) 303-309.

[4] H.L. Huang, C.T Lee, and H.Y. Lee, Performance improvement mechanisms of P3HT: PCBM inverted polymer solar cells using extra PCBM and extra P3HT interfacial layers, Org. Elec. 21 (2015) 126-131.

[5] R. Søndergaard, M. Hösel, D. Angmo, T.T. Larsen-Olsen and F.C. Krebs, Roll-to-roll fabrication of polymer solar cells, Mater. today 15(2012) 36–49

[6] K. Kawano, J. Sakai, M. Yahir and C. Adachi, Effect of solvent on fabrication of active layers in organic solar cells based on poly (3-hexylthiophene) and fullerene derivatives, Sol. Eng. Mater. and Sol. Cell. 93 (2009) 514-518.

[7] M.N. Yusli, T.W. Yun, and K. Sulaiman, Solvent effect on the thin film formation of polymeric solar cells, Mater. Lett. 63 (2009) 2691-2694.

[8] F. Zhang, K.G. Jespersen, C. Björström, M. Svensson, M.R. Andersson, V. Sundström, K. Magnusson, E. Moons, A. Yartsev and O. Inganäs, Influence of solvent mixing on the morphology and performance of solar cells based on polyfluorene copolymer/fullerene blends, Adv. Funct. Mater.16 (2006) 667-674.

[9] V.D. Mihailetchi, H. Xie, B. de Boer, L.M. Popescu, J.C. Hummelen, P.W. Blom and L.J.A Koster, Origin of the enhanced performance in poly (3-hexylthiophene):[6, 6]-phenyl C~ 6~ 1-butyric acid methyl ester solar cells upon slow drying of the active layer, Appl. Phys. Lett. 89 (2006) 12107.

[10] B. Kadem, A. Hassan and W. Cranton, Efficient P3HT: PCBM bulk heterojunction organic solar cells; effect of post deposition thermal treatment. J. Mater. Sci.: Mater. in Elec. 27 (2016) 7038-7048.

[11] M.A. Green, K. Emery, Y. Hishikawa, W. Warta and E.D. Dunlop, Solar cell efficiency tables (Version 48). Prog. in Photovolt.: Res. and Appl. (2016) 905-913.

[12] K. Kim, J. Liu, M.A. Namboothiry and D.L. Carroll, Roles of donor and acceptor nanodomains in 6% efficient thermally annealed polymer photovoltaics, Appl. Phys. Lett. 90 (2007) 163511.

[13] A.J. Moulé and K. Meerholz, Controlling morphology in polymer–fullerene mixtures, Adv. Mater. 20 (2008) 240-245.

[14] M.S. Ryu, J.H. Hyuk and J. Jang, Effects of thermal annealing of polymer: fullerene photovoltaic solar cells for high efficiency, Curr. Appl. Phys. 10 (2010) S206-S209.

[15] B. Kadem, M. Al-hashimi and A. Hassan, The effect of solution processing on the power conversion efficiency of P3HT-based organic solar cells, Eng. Procedia. 50 (2014) 237-245.

[16] B. Kadem, A. Hassan and W. Cranton, The effects of organic solvents and their cosolvents on the optical, structural, morphological of P3HT: PCBM organic solar cells, In Technologies and Materials for Renewable Energy, Environment and Sustainability (TMREES), vol. 1758, no. 1, p. 020006. AIP Publishing, 2016.
[17] B. Kadem, A. Hassan and W. Cranton, Performance optimization of P3HT: PCBM solar cells by controlling active layer thickness. In: 31st European Photovoltaic Solar Energy Conference and Exhibition- Hamburg/Germany (2015): 1090-1094.
[18] B. Kadem, A. Hassan and W. Cranton, P3HT:PCBM-based organic solar cells: the effects of different PCBM derivatives. In: 32nd European Photovoltaic Solar Energy Conference and Exhibition-Munich/Germany (2016): 1332-1337.
[19] B. Kadem, A. Hassan and W. Cranton, Enhancement of power conversion efficiency of P3HT: PCBM solar cell using solution processed Alq3 film as electron transport layer, J. Mater. Sci.: Mater. in Elec. 26 (2015) 3976-3983.
[20] B. Kadem, W. Cranton and A. Hassan, Metal salt modified PEDOT: PSS as anode buffer layer and its effect on power conversion efficiency of organic solar cells, Org. Elec. 24 (2015) 73-79.
[21] G. Yue, J. Wu, Y. Xiao, H. Ye, J. Lin and M. Huang, Flexible dye-sensitized solar cell based on PCBM/P3HT heterojunction, Chin. Sci. Bull. 56 (2011) 325-330.
[22] J. Gasiorowski, R. Menon, K. Hingerl, M. Dachev and N.S. Sariciftci, Surface morphology, optical properties and conductivity changes of poly (3, 4-ethylenedioxythiophene): poly (styrene sulfonate) by using additives, Thin Sold Film 536 (2013) 211-215.
[23] Y.C. Chao, Y.H. Lin, C.Y. Lin, F.M Zhan and Y.Z. Huang, Improved light trapping in polymer solar cells by light diffusion ink. J. Phys. D: Appl. Phys. 47 (2014) 105102.
[24] V.E. Ferry, M.A. Verschuuren, H.B. Li, E. Verhagen, R.J. Walters, R.E. Schropp, H.A. Atwater and A. Polman, Light trapping in ultrathin plasmonic solar cells. Opt. Express. 18 (2010) A237.
[25] L. Zeng, P. Bermel, Y. Yi, B.A. Alamariu, K.A. Broderick, J. Liu, C. Hong, X. Duan, J. Joannopoulos and L.C. Kimerling, Demonstration of enhanced absorption in thin film Si solar cells with textured photonic crystal back reflector, Appl. Phys. Lett. 93 (2008) 221105.
[26] C.E. Petoukhoff and D.M. O'Carroll, Absorption-induced scattering and surface plasmon out-coupling from absorber-coated plasmonic metasurfaces, Nat. commun. 6 (2015) 7899.
[27] B. Hua, Q. Lin, Q. Zhang and Z. Fan, Efficient photon management with nanostructures for photovoltaics, Nanoscale 5 (2013) 6627-6640.
[28] E. Yablonovitch and G.D. Cody, Intensity enhancement in textured optical sheets for solar cells. IEEE Trans. on Elec. Device. 29 (1982) 300-305.
[29] P.K. Petrova, R.L. Tomova and R.T. Stoycheva-Topalova, Organic Light Emitting Diodes Based on Novel Zn and Al Complexes. In: Seung, H. K. "Organic Light Emitting Diode - Material, Process and Devices". Rijeka, Croatia, InTech, 2011, pp. 161-193.
[30] H. Arwin, M. Poksinski, K. Johansen, Total internal reflection ellipsometry: Principles and applications, Appl. Opt. 43 (2004) 3028-3036.
[31] A. Nabok, A. Tsargorodskaya, A. Hassan and N. Starodub, Total internal reflection ellipsometry and SPR detection of low molecular weight environmental toxins, Appl. Surf. Sci. 246 (2005) 381-386.
[32] A. Baba, N. Aoki, K. Shinbo, K. Kato and F. Kaneko, Grating-coupled surface plasmon enhanced short-circuit current in organic thin-film photovoltaic cells. ACS appl. Mater. and interface. 3 (2011) 2080-2084.

[33] [M. Raïssi, L. Vignau, and B. Ratier, Enhancing the short-circuit current, efficiency of inverted organic solar cells using tetra sulfonic copper phthalocyanine (TS-CuPc) as electron transporting layer. Organic Electronics, 15 (2014) 913-919.]
[34] C.W. Chu, H. Yang, W.J. Hou, J. Huang, G. Li and Y. Yang, Control of the nanoscale crystallinity and phase separation in polymer solar cells, Appl. Phys. Lett. 92 (2008) 103306.
[35] Dibb, G. F. A., Jamieson, F. C., Maurano, A., Nelson, J. & Durrant, J. R., Limits on the Fill Factor in Organic Photovoltaics: Distinguishing Nongeminate and Geminate Recombination Mechanisms, J. Phys. Chem. Lett. 4 (2013): 803-808.
[36] V.A. Trukhanov, V.V. Bruevich and D.Y. Paraschuk, Fill factor in organic solar cells can exceed the Shockley-Queisser limit. Sci. Rep.5 (2014) Article number: 11478.
[37] C.J. Brabec, Origin of the open circuit voltage of plastic solar cells. Adv. Funct. Mater. 11 (2001) 374-380.
[38] M.C. Scharber, D. Mühlbacher, M. Koppe, P. Denk, C. Waldauf, Design rules for donors in bulk-heterojunction solar cells - Towards 10% energy-conversion efficiency, Adv. Mater.18 (2006) 789-794.
[39] D.N. Congreve, J. Lee, N.J. Thompson, E. Hontz, S.R. Yost, P.D. Reusswig, M.E. Bahlke, S. Reineke, T. Van-Voorhis and M.A. Baldo, External Quantum Efficiency Above 100% in a Singlet-Exciton-Fission–Based Organic Photovoltaic Cell, Sci. 340 (2013) 334–337.
[40] Ö. Güllü, Ş. Aydoğan, and A. Türüt, High barrier Schottky diode with organic interlayer. Solid State Commun. 152 (2012) 381-385.
[41] C. Liu, X. Yong and Y.Y. Noh, Contact engineering in organic field-effect transistors, Mater.Today. 18 (2015) 79-96.
[42] W. Ma, C. Yang, X. Gong, K. Lee and A.J. Heeger, Thermally Stable, Efficient Polymer Solar Cells with Nanoscale Control of the Interpenetrating Network Morphology. Adv. Funct. Mater. 15 (2005) 1617-1622.
[43] J. Y. Kim, S. H. Kim, H. H. Lee, K. Lee, W. Ma, X. Gong and A. J. Heeger. New Architecture for high-efficiency polymer photovoltaic cells using solution-based titanium oxide as an optical spacer. Advanced materials, 18 (2006) 572-576.
[44] J. Bisquert and G. Garcia-Belmonte, On Voltage, Photovoltage, and Photocurrent in Bulk Heterojunction. J. Phys. Chem. Lett. 2 (2011) 1950-1964.
[45] Y. Peng, L. Zhang and T.L. Andrew, High open-circuit voltage, high fill factor single-junction organic solar cells, Appl. Phys. Lett.105 (2014) 083304.
[46] B. Ray and M.A. Alam, Achieving Fill Factor Above 80% in Organic Solar Cells by Charged Interface. In Photovoltaic Specialists Conference (PVSC), Volume 2, 2012 IEEE 38th (pp. 1-8). IEEE.
[47] D. Meng, D. Sun, D., C. Zhong, T. Liu, B. Fan, L. Huo, Y. Li, W. Jiang, H. Choi, T. Kim and J.Y. Kim, High-Performance Solution-Processed Non-Fullerene Organic Solar Cells Based on Selenophene-Containing Perylene Bisimide Acceptor. J. Am. Chem. Soc. 138 (2016) 375-380.
[48] Y. Liang, Z. Xu, J. Xia, S.T. Tsai, Y. Wu, G. Li, C. Ray and L. Yu, For the bright future-bulk heterojunction polymer solar cells with power conversion efficiency of 7.4%. Adv. Mater. 22 (2010): E135–E138.

Figure captions

Fig. 1: P3HT:PCBM OSC device structure employing complete device processing

Fig. 2: UV-visible absorption and transmittance spectra for the investigated layers

Fig.3: The proposed light trapping mechanism and scattered light from the ITO/LiCl-treated PEDOT:PSS layer

Fig. 4: A SEM image of the PEDOT:PSS layer treated with LiCl

Fig.5: An AFM image representing the morphology of the PEDOT:PSS layer treated with LiCl

Fig. 6: TIRE spectra for the complete device

Fig. **7**: J-V characteristics of the reference and completely processed devices

Fig. 8: IPCE curves of the reference and completely processed devices

Fig. 9: C-V measurements of the completely processed devices

Table 1: Dark and the illuminated parameters for the reference and complete devices

	Illuminated				Dark				
	V_{oc} (V)	J_{sc} (mA.cm^{-2})	FF (%)	PCE (%)	n	ϕ_B (eV)		V_{bi} (V)	R_s (Ω)
						I-V	C-V		
Reference	0.62	11.9	53	3.92	-	-	-	-	-
Average (3 devices)	0.62±0.1	16.4±0.2	70±1	6.95±0.05	-	-	-	-	-
Best device	0.61	16.2	71	7	1.6	0.86	0.86	0.52	45

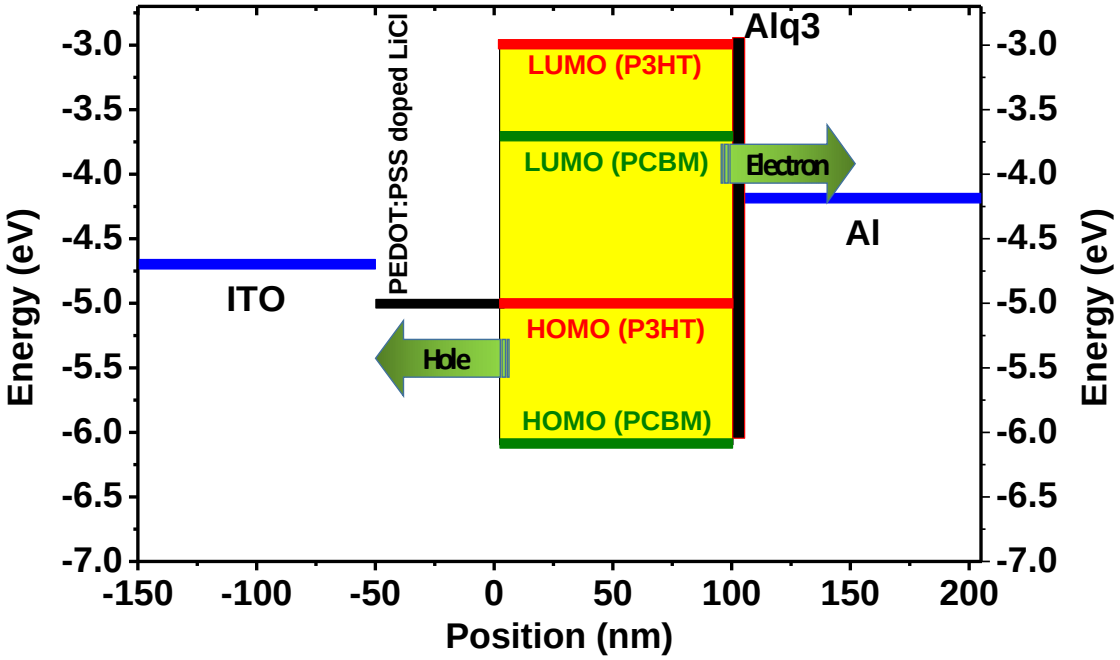

Fig. 1: P3HT:PCBM OSC device structure employing complete device processing

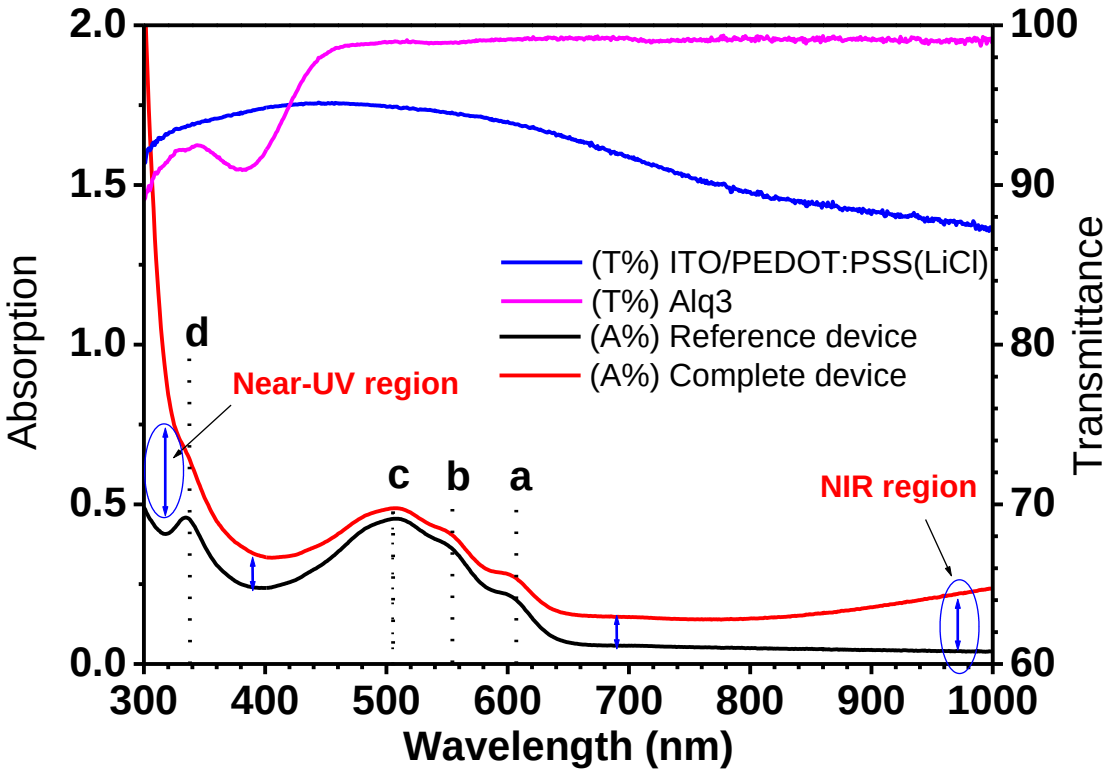

Fig. 2: UV-visible absorption and transmittance spectra for the investigated layers

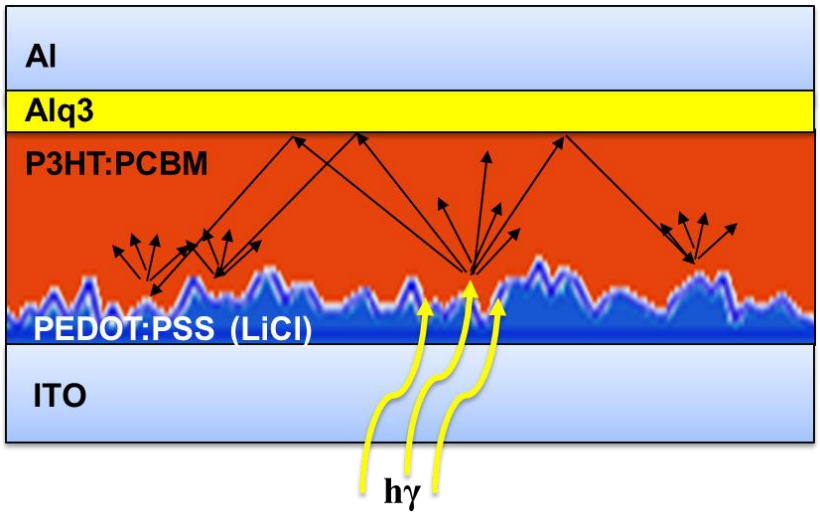

Fig.3: The proposed light trapping mechanism and scattered light from the ITO/LiCl-treated PEDOT:PSS layer

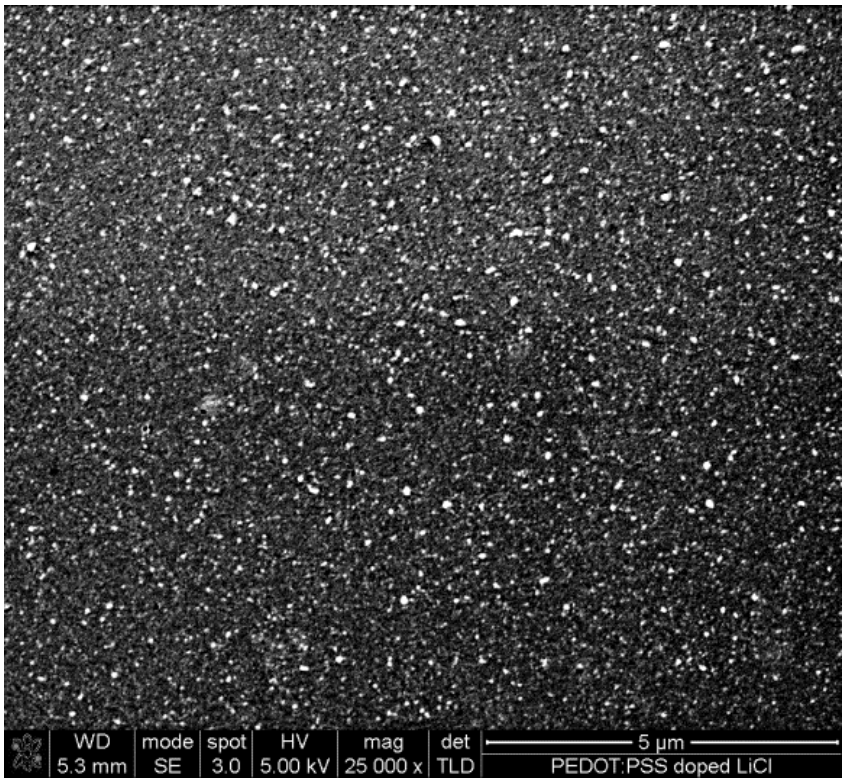

Fig. 4: A SEM image of the PEDOT:PSS layer treated with LiCl

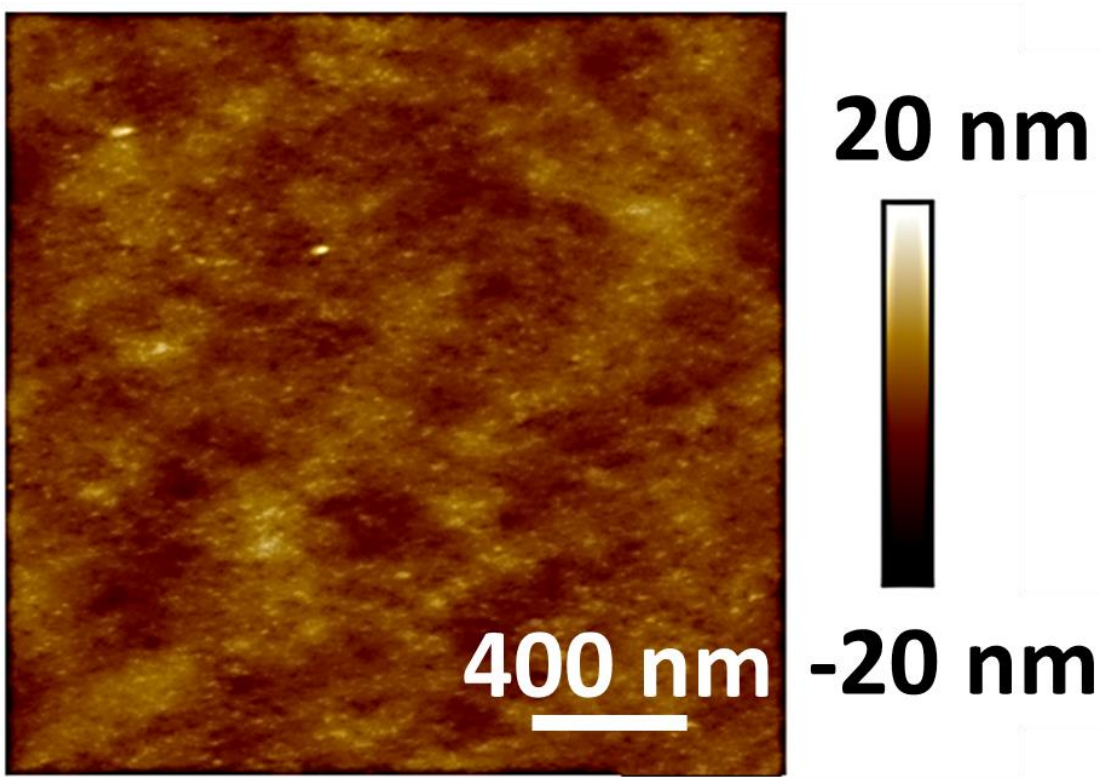

Fig.5: An AFM image representing the morphology of the PEDOT:PSS layer treated with LiCl

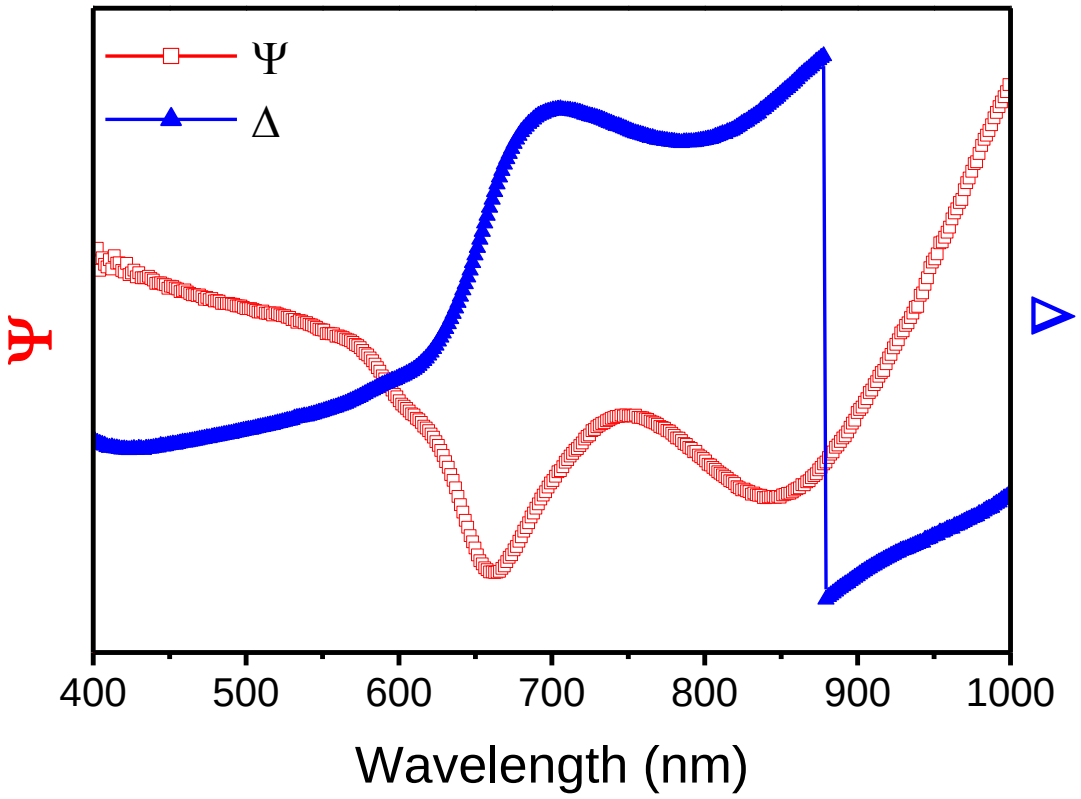

Fig. 6: TIRE spectra for the complete device

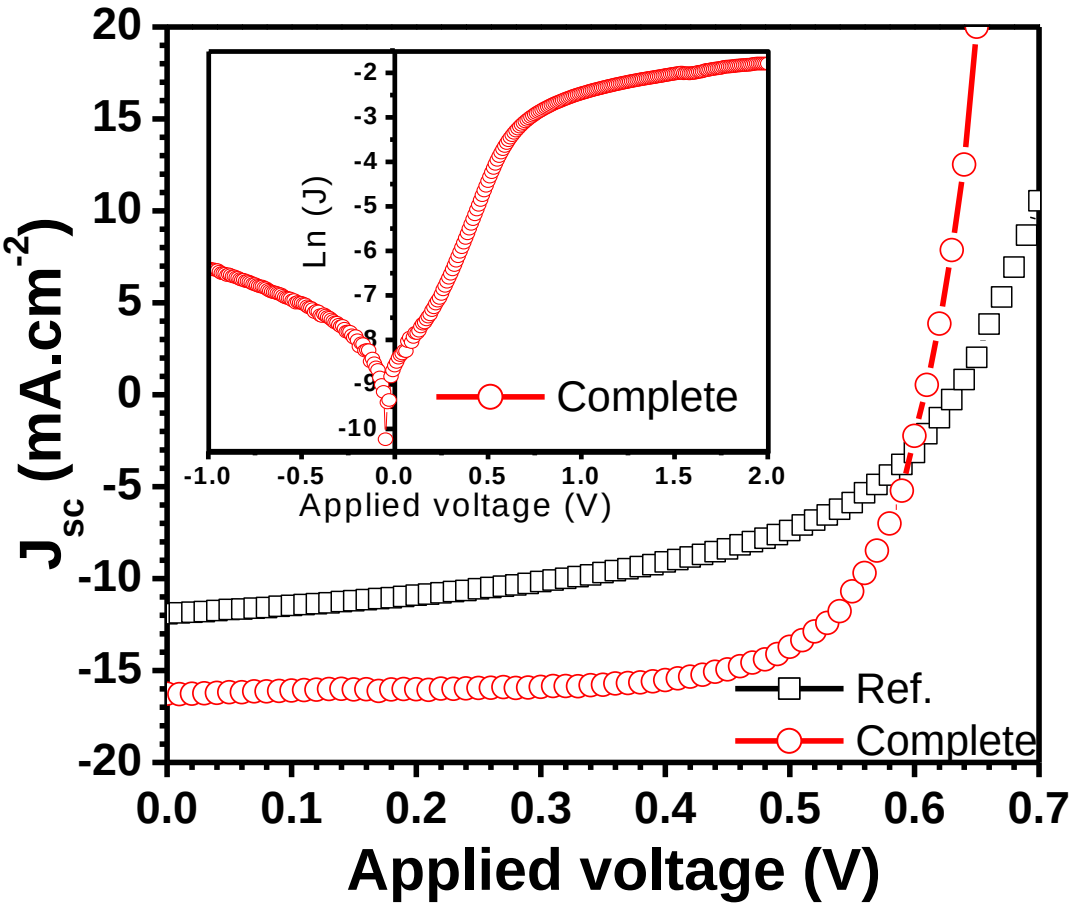

Fig. 7: J-V characteristics of the reference and completely processed devices

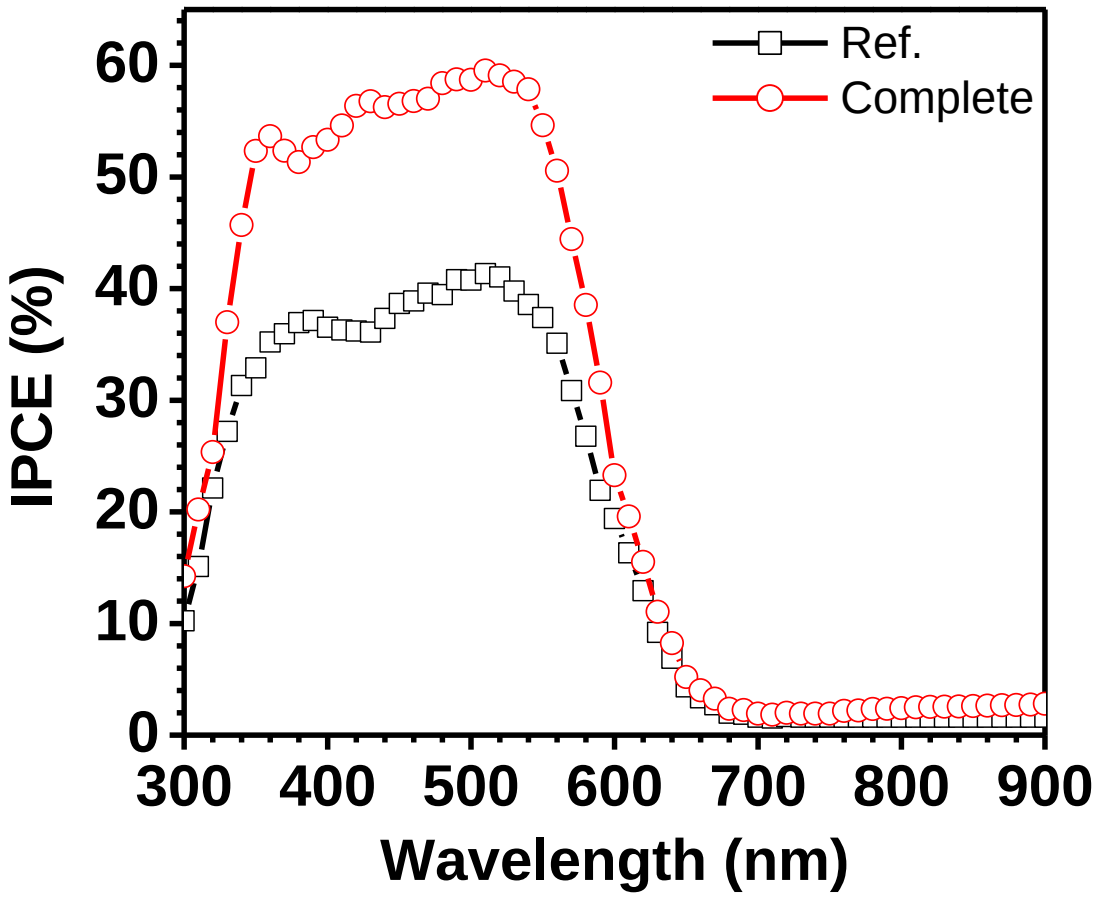

Fig. 8: IPCE curves of the reference and completely processed devices

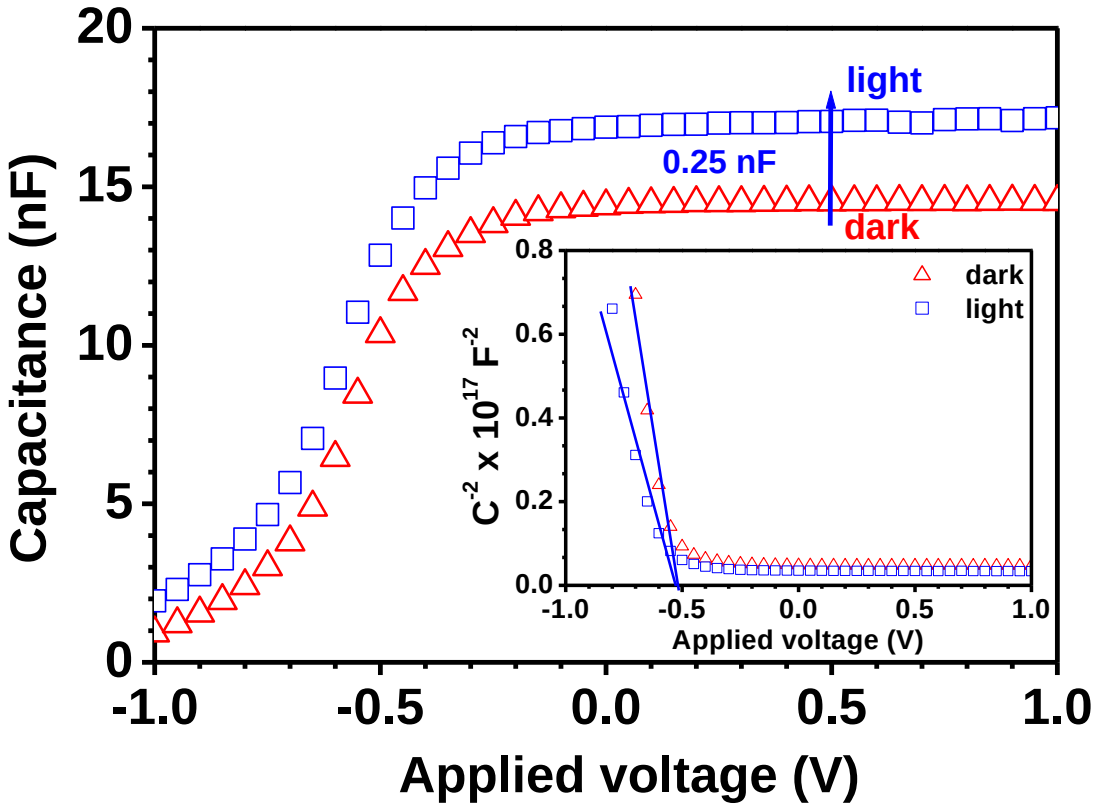

Fig. 9: C-V measurements of the completely processed devices